J. Mech. Phys. Solids 152 (2021) 104409

Contents lists available at ScienceDirect

Journal of the Mechanics and Physics of Solids

journal homepage: www.elsevier.com/locate/jmps

Bounds on the in-plane Poisson's ratios and the in-plane linear and area compressibilities for sheet crystals

Enlai Gao [a,c], Ruishan Li [a], Shaoli Fang [b], Qian Shao [a,*], Ray H. Baughman [b,*]

[a] Department of Engineering Mechanics, School of Civil Engineering, Wuhan University, Wuhan, Hubei 430072, China
[b] Alan G. MacDiarmid NanoTech Institute, The University of Texas at Dallas, Richardson, TX 75080, USA
[c] State Key Laboratory of Water Resources and Hydropower Engineering Science, Wuhan University, Wuhan 430072, China

ARTICLE INFO

Keywords:
Sheets
Auxetic crystals
Negative Poisson's ratios
Linear compressibilities
Area compressibilities

ABSTRACT

It is well known that the Poisson's ratios for 3D isotropic elastic materials vary from -1 to +1/2. These results provide reference points for comparing the Poisson's ratios of anisotropic elastic materials. Sheet crystals (SCs) with remarkably anisotropic structures, in which sheet planes do not intersect, have recently attracted major fundamental and practical interest, while the bounds on the in-plane Poisson's ratios and linear and area compressibilities have not been generically established. Based on the theory of elasticity, we here predict the fundamental bounds on the in-plane Poisson's ratios and linear and area compressibilities for SCs of any crystal system. These predictions are well supported by a data-driven investigation of numerically generated elastic tensors, elastic tensors from first principles calculations for both 2D and 3D SCs, and experimentally measured elastic tensors for 3D SCs. Based on these findings, the range of 2D and 3D SC materials that increase density or planar area or maintain constant density or planar area when stretched, and increase a dimension or planar area when hydrostatically compressed is established for special applications. This work provides fundamental insights and guidelines for the discovery, understanding, and applications of SCs having these properties in tensile strain and hydrostatic pressure environments.

1. Introduction

The Poisson's ratio of an elastic material is the negative ratio of transverse strain to applied axial strain. This Poisson's ratio is a fundamental metric for elastic behavior, as well as a key factor for mechanically-induced density changes and other properties, like the toughness of solids (Greaves et al., 2011; Huang and Chen, 2016; Shivers et al., 2020). The Poisson's ratios of many common materials, such as isotropic polycrystalline metals, polymers and ceramics, are between 0 and 1/2, while some materials can have a negative Poisson's ratio. Such materials with a negative Poisson's ratio are called 'auxetic' (Evans et al., 1991). A host of auxetic materials are well known, such as polymeric foams (Lakes, 1987), cellular structures (Choi and Lakes, 1992), hinged frameworks (Lakes, 1993), origami structures (Pratapa et al., 2019; Schenk and Guest, 2013; Wei et al., 2013), carbon nanotube sheets (Hall et al., 2008), graphene sheets (Gao et al., 2018b; Wen et al., 2019), and metallic sheets (Taylor et al., 2014). These materials are interesting for a wide range of applications, such as enhancing indentation resistance, toughness, and shear resistance (Greaves et al., 2011).

The Poisson's ratios for three-dimensional (3D) isotropic elastic materials are well known to vary from the lower bound of −1 to the

* Corresponding authors.
E-mail addresses: qian.shao@whu.edu.cn (Q. Shao), ray.baughman@utdallas.edu (R.H. Baughman).

https://doi.org/10.1016/j.jmps.2021.104409
Received 22 September 2020; Received in revised form 21 March 2021; Accepted 21 March 2021
Available online 1 April 2021

upper bound of 1/2. This constraint arises from the requirement that their elastic moduli are positive. Also, it is well-known that the upper bound on the Poisson's ratio for the 2D case of 3D isotropic materials, where only in-plane strains are considered, is 1 (Muskhelishvili, 1953; Thorpe and Jasiuk, 1992), which is for an incompressible material. In contrast to isotropic materials, 3D anisotropic materials can have extended bounds on the Poisson's ratios, which depend on the symmetry of the structure (Boulanger and Hayes, 1998; Lempriere, 1968; Ting, 2004; Ting and Barnett, 2005; Ting and Chen, 2005). Remarkably, Ting and Chen (2005) have proven that the Poisson's ratios for anisotropic elastic materials are unbounded, i.e. can have arbitrarily large positive or negative values. The well-established bounds on the Poisson's ratios for 3D crystals of different symmetries provide guidelines for the design and fabrication of crystals having a wide range of Poisson's ratios. Sheet crystals (SCs) having non-intersecting sheets have recently become a great interest (Geim and Novoselov, 2007; Gogotsi and Anasori, 2019), especially their in-plane mechanical properties. Because of the crystal symmetry and the anisotropic nature of bonding, SCs have restrictions on the obtainable properties, such as in-plane Poisson's ratios and linear and area compressibilities.

The large family of presently investigated SCs includes some very important crystals, such as biological β-sheet crystals in proteins and crystals that can be exfoliated into two-dimensional (2D) sheets (Gao et al., 2018a; Yang et al., 2018). SCs can have negative in-plane Poisson's ratios, and some can have negative in-plane linear or area compressibilities. A negative in-plane linear compressibility means that a hydrostatic pressure causes an increase of an in-plane linear dimension of the SC, and a negative in-plane area compressibility means that a hydrostatic pressure causes an increase of the area in the SC plane. Inversely, the application of a uniaxial tensile stress in a direction of negative linear compressibility causes a decrease of volume. Also, the application of an equi-biaxial tensile stress to a plane having a negative area compressibility causes a volume decrease. These mechanical properties are especially important for interfacial engineering in composites and predicting the effects of strains on properties (Greaves et al., 2011; Hall et al., 2008; Wen et al., 2019).

The in-plane Poisson's ratios (ν_{12}, the negative ratio of the in-plane lateral strain in direction 2 to the in-plane tensile strain in direction 1 that produces this lateral strain) of SCs have been extensively investigated, especially for SCs having negative Poisson's ratios (Gibson and Ashby, 1999; Gibson et al., 1982; Grima et al., 2018, 2015; Jiang et al., 2016; Jiang and Park, 2014; Jiang et al., 2016; Wan et al., 2017); (Gao, Liu and Tomanek, 2018b). As early pioneers, Gibson et al. (Gibson and Ashby, 1999; Gibson et al., 1982) theoretically derived the effective elastic constants of 2D honeycombs, and investigated the mechanical properties of honeycomb structures under compression-tension and shearing loads, including negative Poisson's ratios. Bowick et al. (2001) reported that a negative Poisson's ratio is a universal property of self-avoiding fixed-connectivity membranes. Additionally, considerable effort has been devoted to the study of negative Poisson's ratios in graphene (Grima et al., 2018, 2015; Jiang et al., 2016; Jiang and Park, 2016; Qin et al., 2017), graphene-related materials (Wen et al., 2019), and origami based metamaterials (Eidini and Paulino, 2015; Lv et al., 2014; Pratapa et al., 2019; Schenk and Guest, 2013; Yasuda and Yang, 2015). The elastic responses of hexagonal SCs are isotropic within the plane because of the in-plane rotational symmetry (Nye, 1957). For example, the hexagonal sheet structures of the Mo_2C MXene (Mortazavi et al., 2017), graphene (Gao et al., 2018a), MoS_2 (Gao et al., 2018a), β-graphyne (Puigdollers et al., 2016), and α-graphyne (Puigdollers, Alonso and Gamallo, 2016) have isotropic ν_{12} values of −0.15, 0.15, 0.30, 0.67, and 0.87, respectively. In addition, Grima and co-workers (Grima et al., 2015) found that graphene can be converted into a wrinkled sheet structure by randomly removing carbons, which enables the tuning of the in-plane Poisson's ratio. If atomic defects are distributed in special arrangements, graphene sheets can exhibit large negative in-plane Poisson's ratios (Grima et al., 2018). Wan et al. (2017) reported that the in-plane Poisson's ratios of individual graphene oxide sheets can be changed by modifying its degree of oxidation, thereby providing a negative in-plane Poisson's ratio of −0.57 for fully oxidized graphene. Qin et al. (2017) found that the Poisson's ratio of rippled graphene decreases upon increasing the ratio between ripple amplitude over wavelength, and a negative Poisson's ratio of −0.38 was observed. These and other publications indicate that negative in-plane Poisson's ratios can be produced for 2D SCs by either introducing appropriate defects or exploiting thermally or mechanically induced ripples. By considering a wide range of force constants for bond stretching, angle bending, and coupling coefficients, Jiang et al. (2016) reported that graphene has an intrinsic negative in-plane Poisson's ratio for certain combinations of these coupling coefficients. In addition to negative Poisson's ratios, unusually large positive in-plane Poisson's ratios have been reported for SCs. For example, in-plane Poisson's ratios of 0.87 and 0.67 were predicted by first principles calculations for α-graphyne and β-graphyne, respectively (Puigdollers, Alonso and Gamallo, 2016). Moreover, as reported in computational 2D materials database (C2DB, https://cmr.fysik.dtu.dk/) (Haastrup et al., 2018) and the materials project database (MPDB, https://materialsproject.org/) (de Jong et al., 2015), some 2D and 3D SCs have in-plane Poisson's ratios larger than 1. Hence, the reported in-plane Poisson's ratio for SCs can be negative, zero, positive, which is significantly beyond the bounds for 2D and 3D isotropic materials.

The in-plane hydrostatic linear compressibilities and area compressibilities of SCs, which are closely related with the in-plane Poisson's ratios, can result in fascinating properties. For example, a negative in-plane linear compressibility implies that stretching the crystal along the direction of a negative in-plane linear compressibility causes the crystal density to increase (i.e., the crystal is stretch densified) (Baughman et al., 1998). Also, negative in-plane area compressibilities can result that an equibiaxial stretch to a plane having a negative area compressibility causes a volume decrease. Uniaxial stretch or biaxial stretch mean the application of uniaxial elongation or biaxial elongation in the applied stress direction or directions, respectively. In other directions, materials can freely deform as described by the elastic tensor. Hence, a material that is uniaxially or biaxially stretched can undergo dimensional changes in the other directions. These fascinating properties can be useful for many important sensors and high pressure applications (Baughman et al., 1998). However, the bounds of the in-plane Poisson's ratios and the linear and area compressibilities for SCs have not been established, which limits thinking for the design, fabrication, and application of SCs.

The present goal is to establish the bounds on the in-plane Poisson's ratios and linear and area compressibilities for SCs. First, based on the theory of elasticity, we predict the bounds on the in-plane Poisson's ratios and the in-plane linear and area compressibilities for

crystal systems compatible with SCs having non-intersecting sheet planes. These include triclinic, monoclinic, orthorhombic, tetragonal, trigonal, and hexagonal SCs. The predictions show that as the in-plane symmetry of SCs increases, the permitted bounds on the in-plane Poisson's ratios and linear and area compressibilities for SCs become narrow. Afterwards, we did a data-driven investigation of numerically generated elastic tensors, elastic tensors derived from first principles calculations, and experimentally measured elastic tensors to evaluate the bounds on the in-plane Poisson's ratios and linear and area compressibilities for SCs, all of which support the predictions.

2. Results and discussion

2.1. Theoretical prediction

For a Cartesian system x_i ($i = 1, 2, 3$), the mechanical behavior of an elastic solid can be described by the generalized Hooke's law $\boldsymbol{\sigma} = \mathbf{C}\varepsilon$, where $\boldsymbol{\sigma} = [\sigma_{11}, \sigma_{22}, \sigma_{33}, \sigma_{23}, \sigma_{13}, \sigma_{12}]^{\mathrm{T}}$ and $\boldsymbol{\varepsilon} = [\varepsilon_{11}, \varepsilon_{22}, \varepsilon_{33}, 2\varepsilon_{23}, 2\varepsilon_{13}, 2\varepsilon_{12}]^{\mathrm{T}}$ are the stress and strain vectors, respectively, and $\mathbf{C}$ is the stiffness matrix. The strain energy density of the solid is given by $W = 1/2\boldsymbol{\sigma}^{\mathrm{T}}\boldsymbol{\varepsilon} = 1/2\boldsymbol{\sigma}^{\mathrm{T}}\mathbf{S}\sigma$, where $\mathbf{S} = \mathbf{C}^{-1}$ is the compliance matrix. The strain energy density, as the sum of work done by all stress components, must be positive. Therefore, the compliance matrix (or stiffness matrix) should be positive-definite, which requires all principal minors or eigenvalues to be positive:

$$s_{11} > 0, \begin{vmatrix} s_{11} & s_{12} \\ s_{12} & s_{22} \end{vmatrix} > 0, \text{ and } \begin{vmatrix} s_{11} & s_{12} & s_{13} \\ s_{12} & s_{22} & s_{23} \\ s_{13} & s_{23} & s_{33} \end{vmatrix} > 0 \tag{1}$$

where $s_{ii} = 1/E_i$ and $s_{ij} = -\nu_{ij}/E_i = -\nu_{ji}/E_j$ ($i,j = 1,2,3$, and $i \neq j$). Here E_i denotes the Young's modulus in the x_i-direction and ν_{ij} is the Poisson's ratio. Substituting these notations into Eq. (1) leads to

$$\nu_{12}\nu_{21} < 1, \tag{2}$$

and

$$\nu_{12}\nu_{21} + \nu_{13}\nu_{31} + \nu_{23}\nu_{32} + 2\nu_{21}\nu_{32}\nu_{13} < 1, \tag{3}$$

where the indices 1 and 2 are for orthogonal in-plane directions and the index 3 is for an orthogonal perpendicular direction (Fig. 1).

Any elastic solid must satisfy the above conditions. Furthermore, we consider a hydrostatic pressure applied to the elastic solid. The corresponding linear compressibility in the x_1-direction and the area compressibility in the $x_1 - x_2$ plane are $\beta_L = s_{11} + s_{12} + s_{13}$ and $\beta_A = s_{11} + 2s_{12} + s_{13} + s_{22} + s_{23}$, respectively. A negative linear compressibility and a negative area compressibility ($\beta_L < 0$ and $\beta_A < 0$) means, respectively, that:

$$\nu_{12} + \nu_{13} > 1 \tag{4}$$

$$2\nu_{12} + \nu_{13} > 1 + \frac{E_1}{E_2}(1 - \nu_{23}). \tag{5}$$

Materials satisfying Eq. (4) and Eq. (5), respectively, will have a negative linear compressibility in the x_1-direction, and a negative area compressibility in the $x_1 - x_2$ plane.

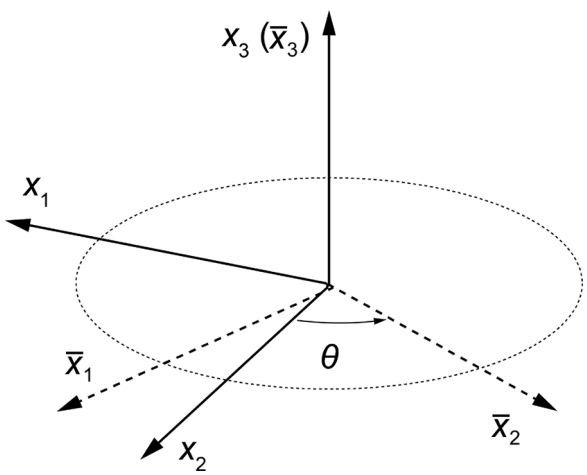

Fig. 1. Illustration of coordinate system rotation along the x_3-axis by an arbitrary angle θ, and the original and new coordinate systems denoted by $x_1 - x_2 - x_3$ and $\bar{x}_1 - \bar{x}_2 - \bar{x}_3$, respectively.

Using Eqs. (2)–(5), the general bounds on the in-plane Poisson's ratios and the in-plane negative linear and area compressibilities are obtained. The symmetry restrictions on compliance matrices for SCs in different crystal systems place additional bounds on the in-plane Poisson's ratios and the linear and area compressibilities. For these discussions, the $x_1 - x_2$ plane is the in-sheet-plane of the SCs, while the x_3-direction is the out-of-plane direction (Fig. 1).

(1) Tetragonal, trigonal, and hexagonal crystals

For tetragonal, trigonal, and hexagonal crystals, $s_{11} = s_{22}$ and $s_{13} = s_{23}$. To investigate the bounds on the in-plane Poisson's ratio for an arbitrary orientation, we rotate the coordinate system along the x_3-axis by an arbitrary angle of θ, resulting in a new coordinate system denoted by $\overline{x}_1$, $\overline{x}_2$, and $\overline{x}_3$ in Fig. 1. The compliance matrix in the rotated coordinate system can be derived from the reference compliance matrix using $\overline{\mathbf{S}} = \mathbf{RSR}^{\mathrm{T}}$, where $\mathbf{R}$ is the rotation matrix defined by

$$\mathbf{R} = \begin{bmatrix} \cos^2\theta & \sin^2\theta & 0 & 0 & 0 & \sin\theta\cos\theta \\ \sin^2\theta & \cos^2\theta & 0 & 0 & 0 & -\sin\theta\cos\theta \\ 0 & 0 & 1 & 0 & 0 & 0 \\ 0 & 0 & 0 & \cos\theta & -\sin\theta & 0 \\ 0 & 0 & 0 & \sin\theta & \cos\theta & 0 \\ -2\sin\theta\cos\theta & 2\sin\theta\cos\theta & 0 & 0 & 0 & \cos^2\theta - \sin^2\theta \end{bmatrix}. \tag{6}$$

The intrinsic symmetry of the compliance tensor for any material leads to $\bar{s}_{12} = \bar{s}_{21}$, $\bar{s}_{13} = \bar{s}_{31}$, and $\bar{s}_{23} = \bar{s}_{32}$. In tetragonal, trigonal, and hexagonal crystals, the components of the rotated compliance tensor have the additional symmetry-related properties, which are that $\bar{s}_{11} = \bar{s}_{22}$ and $\bar{s}_{13} = \bar{s}_{23}$. Given that $\bar{s}_{11} = 1/\overline{E}_1$, $\bar{s}_{22} = 1/\overline{E}_2$, $\bar{s}_{12} = -\bar{\nu}_{21}/\overline{E}_2$, and $\bar{s}_{21} = -\bar{\nu}_{12}/\overline{E}_1$, we can obtain that $\overline{E}_1 = \overline{E}_2$ and $\bar{\nu}_{12} = \bar{\nu}_{21}$. Also given that $\bar{s}_{13} = -\bar{\nu}_{31}/\overline{E}_3$, $\bar{s}_{31} = -\bar{\nu}_{13}/\overline{E}_1$, $\bar{s}_{23} = -\bar{\nu}_{32}/\overline{E}_3$, and $\bar{s}_{32} = -\bar{\nu}_{23}/\overline{E}_2$, we have $\bar{\nu}_{13} = \bar{\nu}_{23}$ and $\bar{\nu}_{31} = \bar{\nu}_{32}$. Eqs. (2) and (3) that define the general bounds on the Poisson's ratios in any elastic solid consists of two conditions. Substituting the above-derived $\bar{\nu}_{12} = \bar{\nu}_{21}$ into Eq. (2) results in the first limit on the in-plane Poisson's ratios for tetragonal, trigonal, and hexagonal crystals,

$$-1 < \bar{\nu}_{12} < 1. \tag{7}$$

Then, substituting above-derived $\bar{\nu}_{12} = \bar{\nu}_{21}$, $\bar{\nu}_{13} = \bar{\nu}_{23}$, and $\bar{\nu}_{31} = \bar{\nu}_{32}$ into Eq. (3), we obtain the second limit on the in-plane Poisson's ratios,

$$\bar{\nu}_{12}^2 + 2\bar{\nu}_{12}\bar{\nu}_{13}^2\frac{\overline{E}_3}{\overline{E}_1} + 2\bar{\nu}_{13}^2\frac{\overline{E}_3}{\overline{E}_1} - 1 < 0, \tag{8}$$

which can be rewritten into the following form,

$$\left(\bar{\nu}_{12} + 1\right)\left(\bar{\nu}_{12} - 1 + 2\bar{\nu}_{13}^2\frac{\overline{E}_3}{\overline{E}_1}\right) < 0. \tag{9}$$

Given that Eq. (7) must be satisfied in any tetragonal, trigonal, or hexagonal crystal, it implies that $\bar{\nu}_{12} + 1 > 0$. Thus the above inequality can be simplified to

$$\bar{\nu}_{12} < 1 - 2\bar{\nu}_{13}^2\frac{\overline{E}_3}{\overline{E}_1}. \tag{10}$$

Therefore, Eqs. (7) and (10) define the bounds on the in-plane Poisson's ratios of tetragonal, trigonal, and hexagonal crystals for arbitrary stretch directions.

Hence, the maximum and minimum in-plane Poisson's ratios must satisfy $-1 < \nu_{\min} \le \nu_{\max} < 1$. Specifically, trigonal and hexagonal crystals provide in-plane isotropy, so that $\bar{s}_{11} = s_{11}$ and $\bar{s}_{12} = s_{12}$. This means that the in-plane Poisson's ratios for arbitrary stretch directions within the sheet plane are equal, and result in $-1 < \nu_{\min} = \nu_{\max} < 1$.

Considering the properties of compliance tensors in tetragonal, trigonal, and hexagonal crystals, to obtain a negative linear compressibility or area compressibility, according to Eqs. (4) and (5), the in-plane and out-of-plane Poisson's ratios should satisfy $\bar{\nu}_{12} + \bar{\nu}_{13} > 1$. Specifically, the linear compressibility in an arbitrary in-plane direction of $\overline{x}_1$ and the area compressibility of an arbitrary $\overline{x}_1$

Table 1
Theoretical bounds on the in-plane Poisson's ratios and the in-plane linear and area compressibilities of SCs in different crystal systems (The 2D case can be seen in Table 2).

Crystal system	General bounds on the Poisson's ratio	Bounds on the in-plane Poisson's ratios	Bounds on the in-plane linear and area compressibilities
Hexagonal Trigonal	$-1 < \bar{\nu}_{12} < 1$, $\bar{\nu}_{12} < 1 - 2\bar{\nu}_{13}^2\overline{E}_3/\overline{E}_1$	$-1 < \nu_{\min} = \nu_{\max} < 1$	$\bar{\beta}_A = 2\bar{\beta}_L > -1/(4\overline{E}_3), \bar{\beta}_L^{\max} = \bar{\beta}_L^{\min}$
Tetragonal	$-1 < \bar{\nu}_{12} < 1$, $\bar{\nu}_{12} < 1 - 2\bar{\nu}_{13}^2\overline{E}_3/\overline{E}_1$	$-1 < \nu_{\min} \le \nu_{\max} < 1$	$\bar{\beta}_A = 2\bar{\beta}_L > -1/(4\overline{E}_3), \bar{\beta}_L^{\max} = \bar{\beta}_L^{\min}$
Orthorhombic Monoclinic Triclinic	$\begin{cases} \bar{\nu}_{12}\bar{\nu}_{21} < 1 \\ \bar{\nu}_{12}\bar{\nu}_{21} + \bar{\nu}_{13}\bar{\nu}_{31} + \\ \bar{\nu}_{23}\bar{\nu}_{32} + 2\bar{\nu}_{21}\bar{\nu}_{32}\bar{\nu}_{13} < 1 \end{cases}$	$\nu_{\max}\nu_{\min} < 1$	$\bar{\beta}_A = \bar{\beta}_L^{\max} + \bar{\beta}_L^{\min} > -1/(4\overline{E}_3)$

$-\bar{x}_2$ plane become $\bar{\beta}_L = (1 - \bar{\nu}_{12} - \bar{\nu}_{13})/\bar{E}_1$ and $\bar{\beta}_A = 2(1 - \bar{\nu}_{12} - \bar{\nu}_{13})/\bar{E}_1$, respectively. The minimum values of $\bar{\beta}_L$ and $\bar{\beta}_A$ are determined by the bounds on the in-plane Poisson's ratios, as shown in Eqs. (7) and **(10)**. When $\bar{\nu}_{12}$ approaches $1 - \bar{E}_1/(8\bar{E}_3)$ and $\bar{\nu}_{13}$ approaches $\bar{E}_1/(4\bar{E}_3)$, $\bar{\beta}_L$ and $\bar{\beta}_A$ reach their lower bounds, which are $-1/(8\bar{E}_3)$ and $-1/(4\bar{E}_3)$, respectively.

Note that the in-plane linear compressibility in these crystal systems is isotropic (one-half of the area compressibility). The bounds on the in-plane Poisson's ratios and the in-plane linear and area compressibilities of tetragonal, trigonal, and hexagonal crystals are summarized in Table 1 and Fig. 2**a**.

(2) Orthorhombic, monoclinic, and triclinic crystals

The components of the compliance tensor related to $\bar{s}_{11}$, $\bar{s}_{22}$, $\bar{s}_{33}$, $\bar{s}_{12}$, $\bar{s}_{23}$, and $\bar{s}_{13}$ have no symmetry-dependent relationships in orthorhombic, monoclinic, and triclinic crystals. Thus, the restrictions on the in-plane and out-of-plane Poisson's ratios are determined by Eqs. (2) **and** (3). For the case that the maximum in-plane Poisson's ratio $\nu_{\max}$ is obtained at the rotated $\bar{x}_1 - \bar{x}_2$ plane, we denote $\nu_{\max} = \bar{\nu}_{12}$ and $\nu'_{\max} = \bar{\nu}_{21}$. According to Eq. (2), we obtain that $\nu_{\max}\nu'_{\max} < 1$. Similarly, for the minimum in-plane Poisson's ratio, we have $\nu_{\min}\nu'_{\min} < 1$. If $\nu_{\max}$ is positive, $\nu_{\min}\nu_{\max} \le \nu'_{\max}\nu_{\max} < 1$ because the condition $\nu_{\min} \le \nu'_{\max}$ must be satisfied. If $\nu_{\max}$ is non-positive, $\nu_{\min}$ must also be non-positive. Given that $\nu'_{\min} \le \nu_{\max}$, we obtain $\nu_{\min}\nu_{\max} \le \nu_{\min}\nu'_{\min} < 1$. Eventually, the maximum and minimum in-plane Poisson's ratios should satisfy $\nu_{\max}\nu_{\min} < 1$. Although the Poisson's ratios for 2D cellular materials were previously found to be unbounded in absolute magnitude (Gibson and Ashby, 1999; Gibson et al., 1982), this additional limit ($\nu_{\max}\nu_{\min} < 1$) on the in-plane Poisson's ratios for SCs was not described.

The region bounded by Eqs. (2)**–(**5**)** exhibit negative in-plane linear and area compressibilities, as shown in Fig. 2**(b)**. To investigate the minimum negative area compressibility, a constrained optimization problem ($\min f(\bar{\nu}_{12}, \bar{\nu}_{13}, \bar{\nu}_{23}) = \bar{\beta}_A \cdot \bar{E}_3$ *s.t.* $\bar{\nu}_{12}\bar{\nu}_{21} < 1$ and $\bar{\nu}_{12}\bar{\nu}_{21} + \bar{\nu}_{13}\bar{\nu}_{31} + \bar{\nu}_{23}\bar{\nu}_{32} + 2\bar{\nu}_{21}\bar{\nu}_{32}\bar{\nu}_{13} < 1$) is solved, and it is found that the linear and area compressibilities should satisfy $\bar{\beta}_A = \bar{\beta}_L^{\max} + \bar{\beta}_L^{\min} > -1/(4\bar{E}_3)$, as summarized in Table 1. Notably, the bounds on the area compressibilities of SCs are independent on the crystal systems, and hence it can be generalized for all materials with positive-definite elastic tensors.

2.2. Data-driven verification

To verify the predicted bounds on the in-plane Poisson's ratios and the in-plane linear and area compressibilities for SCs, elastic tensors were generated by a numerical procedure in the framework of elasticity constraints (see Appendix A for details). Considering the anisotropic nature of SCs, we calculated the maximum and minimum in-plane Poisson's ratios and the in-plane linear and area compressibilities for these numerically generated elastic tensors. The results are shown in Fig. 3**(a)** and Fig. 4**(a, d)** for SCs from different crystal systems, which show that the numerical data agree with the theoretical bounds for each crystal system.

To further verify the predictions of the bounds on the in-plane Poisson's ratios and the in-plane linear and area compressibilities for SCs, we compared the predictions with results obtained from experimentally determined and first principles calculated elastic tensors for 2D and 3D SCs. First, we did a literature survey, and the maximum and minimum in-plane Poisson's ratios for typical 2D SCs are summarized in Table 3. Most of the surveyed 2D SCs have hexagonal lattices, and thus the in-plane Poisson's ratios in all directions are equal ($\nu_{\min} = \nu_{\max}$). The lowest value for the in-plane Poisson's ratio for a 2D SC was found for a MXene (Mo_2C, −0.15), while the highest value was for α-graphyne (+0.87). These extreme values for hexagonal sheets fall within the predicted bounds (−1, 1). In addition, the in-plane Poisson's ratios for 2D SCs in other crystal systems of Table 3 also fall in the theoretical bounds. Notably, Cabras and Brun (2014) proposed hexagonal, triangular and square honeycomb structures with a Poisson's ratio approaching the thermodynamic limit of −1. The underlying physics is a macroscopic non-chiral effect arising from the superposition of clockwise and anticlockwise internal rotations. For comparison, the dominant deformation mechanism of classical honeycomb structures is by extension and bending. For example, as analyzed by Gibson and Ashby (1999), Gibson et al. (1982), the effective behavior of honeycombs with hexagonal lattices is dominated by cell-wall bending. Afterwards, using the computational 2D materials database (C2DB, https://cmr.fysik.dtu.dk/) of elastic tensors for 2D SCs from density functional theory (DFT) calculations (Haastrup et al., 2018), the materials project database (MPDB, https://materialsproject.org/) of elastic tensors for 3D SCs from DFT calculations (de Jong et al., 2015), and the database of experimentally measured elastic tensors for 3D SCs (Every and McCurdy, 1992), Fig. 3**(b–d)** compares the theoretical bounds on the in-plane Poisson's ratios with the minimum and maximum in-plane Poisson's ratios calculated from elastic tensors from DFT calculations for 2D SCs, elastic tensors from DFT calculations for 3D SCs, and measured elastic tensors for 3D SCs. These results show that the bounds of maximum and minimum in-plane Poisson's ratios for 2D SCs and 3D SCs from both calculations and experiments agree well with their predicted bounds. Similar to the in-plane Poisson's ratios, the bounds of maximum and minimum in-plane linear and in-plane area compressibilities for SCs (from both first principles calculations and experiments) agree well

Table 2
Theoretical bounds on the in-plane Poisson's ratios of 2D SCs in different crystal systems.

Crystal system	Bounds on the in-plane Poisson's ratios
Hexagonal Trigonal	$-1 < \nu_{\max} = \nu_{\min} < 1$
Square	$-1 < \nu_{\min} \le \nu_{\max} < 1$
(Centered) Rectangular Oblique	$\nu_{\max}\nu_{\min} < 1$

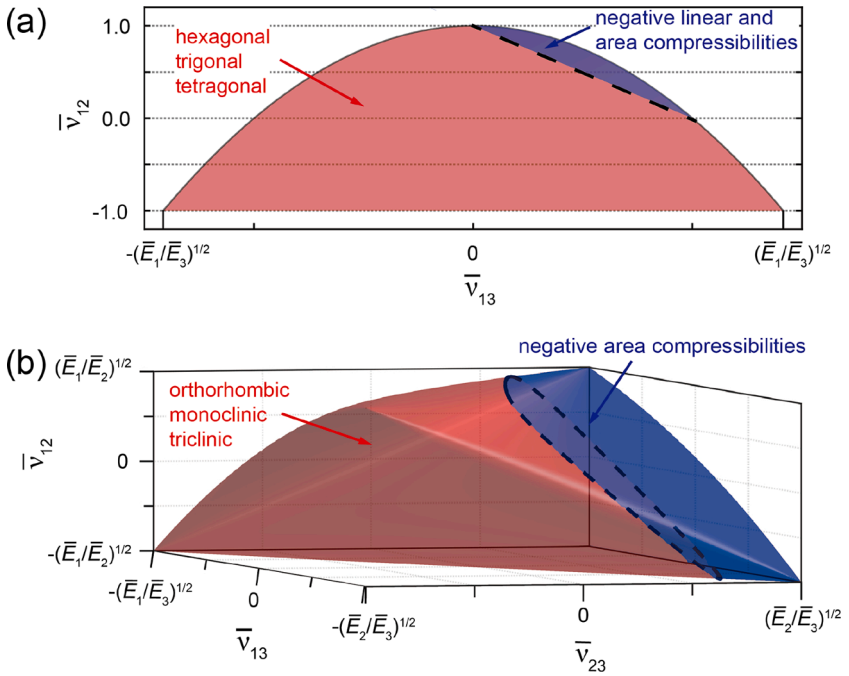

Fig. 2. Theoretical bounds on the Poisson's ratios of SCs of (a) hexagonal, trigonal, and tetragonal crystals and (b) orthorhombic, monoclinic, and triclinic crystals. The regions bounded by the red and blue surfaces represent the permissible range of the Poisson's ratios, while the in-plane negative linear and area compressibilities are obtained when the Poisson's ratios locate in the blue region. (For interpretation of the references to color in this figure legend, the reader is referred to the web version of this article.)

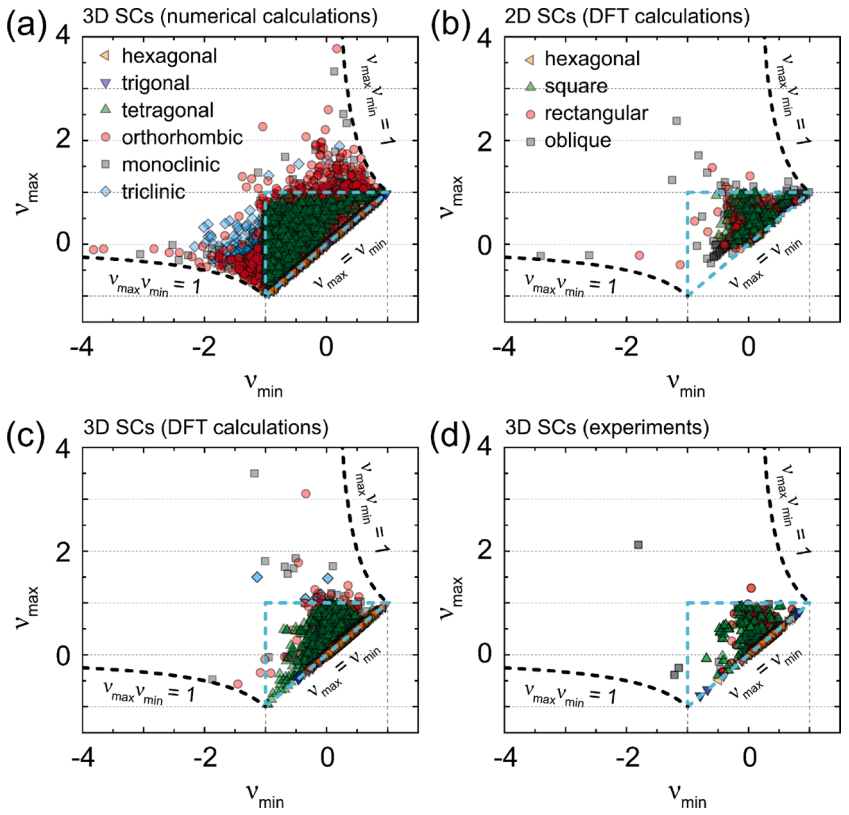

Fig. 3. Bounds on the maximum and minimum in-plane Poisson's ratios calculated from (a) numerically generated elastic tensors for 3D SCs, (b) elastic tensors from first principles calculations for 2D SCs, (c) elastic tensors from first principles calculations for 3D SCs, and (d) experimentally measured elastic tensors for 3D SCs. The dashed lines represent the theoretical bounds on the in-plane Poisson's ratios.

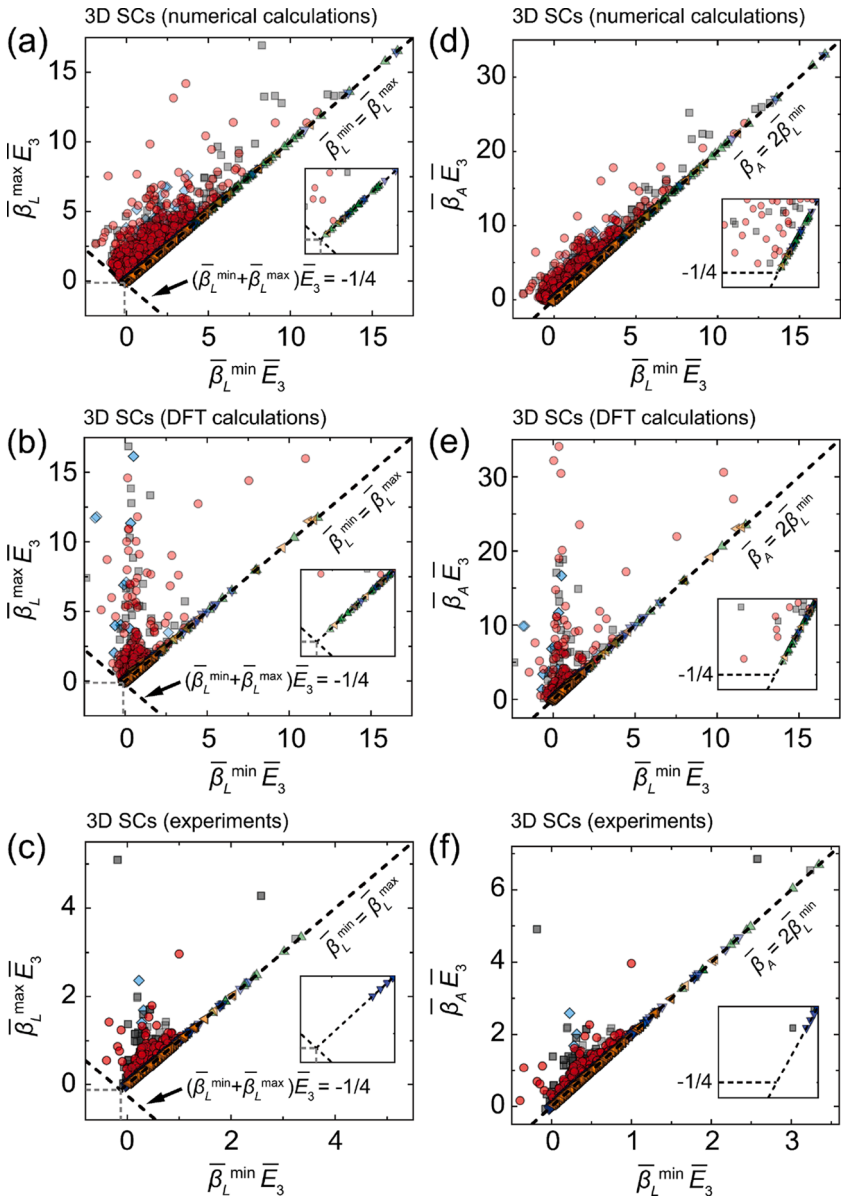

Fig. 4. For hexagonal (orange triangles), trigonal (purple triangles), tetragonal (green triangles), orthorhombic (red dots), monoclinic (gray squares), and triclinic (light blue squares) 3D SCs, the dependence of the maximum in-plane linear compressibility (**a-c**) and the in-plane area compressibility (**d-f**) on the minimum in-plane linear compressibility, where the compressibilities are made non-dimensional by multiplying them by $\overline{E}_3$. These results are from (a, d) numerically generated elastic tensors, (b, e) elastic tensors from first principles calculations, and (c, f) experimentally measured elastic tensors for SCs. The dashed lines and the insets (magnified views of the main figures) show the predicted lower limits on the in-plane linear and area compressibilities. (For interpretation of the references to color in this figure legend, the reader is referred to the web version of this article.)

Table 3
Maximum and minimum in-plane Poisson's ratio for typical 2D SCs.

Material	Crystal systems	ν_{max}	ν_{min}	Refs
Mxene ($Ti_3C_2T_x$)	hexagonal	0.227	0.227	(Fu et al., 2016) (calculations)
Mxene (Ti_2CO_2)	hexagonal	0.312	0.312	(Khaledialidusti et al., 2020) (calculations)
Mxene ($Ti_3C_2O_2$)	hexagonal	0.304	0.304	(Khaledialidusti et al., 2020) (calculations)
Mxene (Mo_2C)	hexagonal	−0.15	−0.15	(Mortazavi et al., 2017) (calculations)
graphene	hexagonal	0.15	0.15	(Gao and Xu, 2015) (calculations)
α-graphyne	hexagonal	0.87	0.87	(A.R. Puigdollers et al., 2016) (calculations)
β-graphyne	hexagonal	0.67	0.67	(A.R. Puigdollers et al., 2016) (calculations)
γ-graphyne	hexagonal	0.42	0.42	(A.R. Puigdollers et al., 2016) (calculations)
h-BN	hexagonal	0.21	0.21	(Gao and Xu, 2015) (calculations)
MoS_2	hexagonal	0.30	0.30	(Gao and Xu, 2015) (calculations)
2D Silica	hexagonal	0.50	0.50	(Gao et al., 2016) (calculations)
Silicene	hexagonal	0.28	0.28	(Gao and Xu, 2015) (calculations)
2D hexagonal lattice	hexagonal	–	−1	(Cabras and Brun, 2014) (theory & exp.)
2D triangular lattice	trigonal	–	−1	(Cabras and Brun, 2014)(theory & exp.)
2D square lattice	square	–	−1	(Cabras and Brun, 2014) (theory & exp.)
Penta-graphene	square	0.068	0.068	(Zhang et al., 2015) (calculations)
Borophene	rectangular	−0.02	−0.04	(Mannix et al., 2015) (calculations)
δ-P	rectangular	0.29	−0.27	(Wang et al., 2017) (calculations)

their predicted bounds [Fig. 4**(a–f)**].

These bounds on the in-plane Poisson's ratios and linear and area compressibilities for SCs provide guidelines for discovering new sheet structures having extreme mechanical behaviors for tuning functional properties. Three types of unusual mechanical properties are bounded for SCs based on the above-mentioned explorations (Figs. 3 **and** 4).

(1) Ordinary sheets increase the sheet area within the plane when uniaxially stretched in any in-plane direction. However, Fig. 3 shows that the in-plane Poisson's ratios for some SCs with orthorhombic, monoclinic, triclinic lattices exceed 1, indicating that the area within the plane decreases during an in-plane stretch for directions having such large in-plane Poisson's ratios. The existence of SCs with unusually large Poisson's ratios means that sheets can be obtained whose in-plane area either decreases with increasing stretch or is stretch invariant. The latter possibility arises for any stretch-area-densified SCs, because there must exist a family of in-plane directions in which the in-plane Poisson's ratio equals 1.

(2) Ordinary materials decrease density when uniaxially stretched in any in-plane direction. A few rare materials, called stretch-densified materials, have directions of negative linear compressibilities in which stretch increases density, while compression decreases it. Similar to the above mentioned area densified properties, the existence of SCs with negative linear compressibility means that sheets can be obtained whose density either increase with increasing stretch or is stretch invariant. The latter possibility arises for any stretch densified SCs, since there must exist a family of in-plane directions in which the linear compressibility vanishes. Table 1 shows that the lower bounds on the linear compressibilities are $-1/(8\bar{E}_3)$ for hexagonal, trigonal, and tetragonal SCs, while there are no bounds on the linear compressibilities for orthorhombic, monoclinic, and triclinic SCs. These conclusions are supported by both calculations and experiments (Fig. 4). It means that the density can be dramatically increased for orthorhombic, monoclinic, triclinic SCs when the stretch is along the direction of an extremely negative linear compressibility.

(3) Ordinary materials decrease the area within all planes when hydrostatically compressed. A few SCs exhibit the reverse behavior – the in-plane area increases when hydrostatically compressed. The theory predicts that the lower bound on the area compressibility for SCs of any lattices is $-1/(4\bar{E}_3)$. Fig. 4 shows that there are some SCs, from both calculations and experiments, that approach the bounds, indicating the predicted extreme behaviors exist in real materials.

These unusual properties of materials, for example, that decrease planar area when stretched, and increase planar area when hydrostatically compressed may be used for some very special applications, for example, high pressure sensors (Baughman et al., 1998;

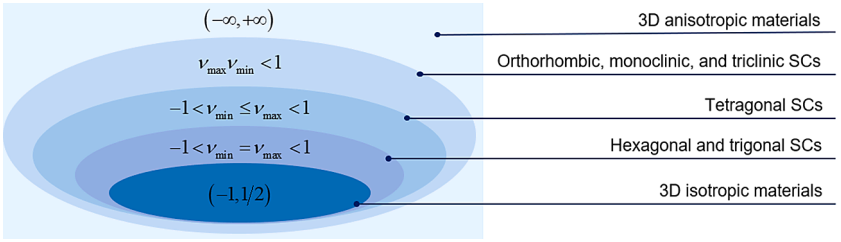

Fig. 5. Schematic illustration of the progressively restricted bounds on the Poisson's ratios for 3D anisotropic materials and 3D isotropic materials, and the bounds on the in-plane Poisson's ratios for SCs in different crystal systems.

Greaves et al., 2011; Huang and Chen, 2016). The bounds on the in-plane Poisson's ratios and linear and area compressibilities provide a reference line for discovering new SCs having extreme mechanical properties for advanced engineering applications.

3. Concluding remarks

It has been long known that the general bounds on Poisson's ratios for 3D isotropic and anisotropic materials are $(-1, 1/2)$ and $(-\infty, +\infty)$, respectively, and the Poisson's ratios for 2D isotropic materials can be higher than 1/2. However, previous work has not considered the effect of crystal symmetry on the allowable Poisson's ratios for the sheet planes of SCs. To fill this gap, this work analyzed all types of 3D and 2D SCs and demarcated the bounds on the in-plane Poisson's ratios and the linear and area compressibilities for SCs in each specific crystal system. As illustrated in Fig. 5, the reduced dimensionality in SCs narrows the permitted bounds on the properties in the sheet planes, which is significantly different from the general bounds for 3D anisotropic materials, because the in-plane properties are confined in a 2D space. The increase of the in-plane symmetry of SCs introduces constraints to the in-plane properties, which also narrows the permitted bounds on the in-plane Poisson's ratios and linear and area compressibilities. The bounds on Poisson's ratios for 3D and 2D materials given in the literature are typically derived exclusively based on theory of elasticity. Considering the requirement of material chemical stability, whether these bounds can be achieved by real materials is questionable. For example, although Young's moduli of materials are unbounded if only considering positive-definiteness of the elastic moduli, the upper bound on the Young's moduli for real bulk materials never exceeds 2000 GPa (the already-known highest Young's modulus for bulk crystals is 1555 GPa for CN_2) (Shao et al., 2021). To address this concern, this work has investigated a large number of extreme Poisson's ratios of real materials from first principles calculations and experimental measurements to verify their theoretical bounds, which indicates that many predicted extreme behaviors of Poisson's ratios do exist in real materials (Fig. 3).

In summary, we predicted the bounds on the in-plane Poisson's ratios and linear and area compressibilities for SCs. The predictions are well supported for numerically generated elastic tensors, first principles calculated elastic tensors, and experimentally measured elastic tensors for SCs. Based on the developed bounds, extreme and unusual mechanical properties of SCs are discussed for some useful applications. These findings presented in this work for in-plane Poisson's ratios and the in-plane linear and area compressibilities for SCs, provide fundamental guidelines for the design, fabrication, and applications of SCs with extreme and unusual mechanical properties.

CRediT authorship contribution statement

Enlai Gao: Conceptualization, Formal analysis, Investigation, Methodology, Visualization, Funding acquisition, Writing – original draft, Writing – review & editing. **Ruishan Li:** Investigation, Visualization. **Shaoli Fang:** Writing – review & editing. **Qian Shao:** Conceptualization, Formal analysis, Investigation, Methodology, Visualization, Funding acquisition, Writing – review & editing. **Ray H. Baughman:** Conceptualization, Formal analysis, Funding acquisition, Supervision, Writing – review & editing.

Declaration of Competing Interest

The authors declare no competing financial or non-financial interests.

Acknowledgments

This work in China was supported by the National Natural Science Foundation of China (11902225 and 11702199). This work in the United States was supported by the Robert A. Welch Foundation grant AT-0029. The numerical calculations in this work have been done on the supercomputing system in the Supercomputing Center of Wuhan University.

Appendix A

Method used for numerically generating the elastic tensors

The elastic tensors were randomly generated using two constraints. The first constraint is that the number of independent elastic constants and the generated tensor must be consistent with the general form of the elastic tensor for each crystal system. The second constraint is that the generated elastic tensor must be positive definite. Herein, the first constraint is only related to the symmetry of crystals, and the second one corresponds to the requirement of mechanical stability. Using a hexagonal crystal as an example, the numerical procedure deployed for generating elastic tensors is as follows:

Step 1: According to the symmetry of the hexagonal crystal, we randomly generated 10^4 stiffness matrices having the following form:

$$\begin{bmatrix} C_{11} & C_{12} & C_{13} & 0 & 0 & 0 \\ C_{12} & C_{11} & C_{13} & 0 & 0 & 0 \\ C_{13} & C_{13} & C_{33} & 0 & 0 & 0 \\ 0 & 0 & 0 & C_{44} & 0 & 0 \\ 0 & 0 & 0 & 0 & C_{44} & 0 \\ 0 & 0 & 0 & 0 & 0 & \frac{C_{11}-C_{12}}{2} \end{bmatrix}.$$

Step 2: For each matrix, we calculated its eigenvalues. Only those matrices whose eigenvalues are all positive were retained and considered as possible elastic tensors.

Step 3: The elastic matrices were rotated along the x_3-axis, to calculate the maximum and minimum in-plane Poisson's ratios and in-plane linear and area compressibilities.

References

Baughman, R.H., Stafstrom, S., Cui, C., Dantas, S.O., 1998. Materials with negative compressibilities in one or more dimensions. Science 279, 1522–1524.

Boulanger, P., Hayes, M., 1998. Poisson's ratio for orthorhombic materials. J. Elast. 50, 87–89.

Bowick, M., Cacciuto, A., Thorleifsson, G., Travesset, A., 2001. Universal negative Poisson ratio of self-avoiding fixed-connectivity membranes. Phys. Rev. Lett. 87, 148103.

Cabras, L., Brun, M., 2014. Auxetic two-dimensional lattices with Poisson's ratio arbitrarily close to −1. Proc. R. Soc. A 470, 20140538.

Choi, J.B., Lakes, R.S., 1992. Non-linear properties of metallic cellular materials with a negative Poisson's ratio. J. Mater. Sci. 27, 5375–5381.

de Jong, M., Chen, W., Angsten, T., Jain, A., Notestine, R., Gamst, A., Sluiter, M., Krishna Ande, C., van der Zwaag, S., Plata, J.J., Toher, C., Curtarolo, S., Ceder, G., Persson, K.A., Asta, M., 2015. Charting the complete elastic properties of inorganic crystalline compounds. Sci. Data 2, 150009.

Eidini, M., Paulino, G.H., 2015. Unraveling metamaterial properties in zigzag-base folded sheets. Sci. Adv. 1, e1500224.

Evans, K.E., Nkansah, M.A., Hutchinson, I.J., Rogers, S.C., 1991. Molecular network design. Nature 353, 124. -124.

Every, A.G., McCurdy, A.K., 1992. Low Frequency Properties of Dielectric crystals, vol. 29a of Landolt-Börnstein, New Series, Group III. Springer. https://doi.org/10.1007/b44185.

Fu, Z.H., Zhang, Q.F., Legut, D., Si, C., Germann, T.C., Lookman, T., Du, S.Y., Francisco, J.S., Zhang, R.F., 2016. Stabilization and strengthening effects of functional groups in two-dimensional titanium carbide. Phys. Rev. B 94.

Gao, E.L., Lin, S.Z., Qin, Z., Buehler, M.J., Feng, X.Q., Xu, Z.P., 2018a. Mechanical exfoliation of two-dimensional materials. J. Mech. Phys. Solids 115, 248–262.

Gao, E.L., Xie, B., Xu, Z.P., 2016. Two-dimensional silica: structural, mechanical properties, and strain-induced band gap tuning. J. Appl. Phys. 119, 014301.

Gao, E.L., Xu, Z.P., 2015. Thin-shell thickness of two-dimensional materials. J. Appl. Mech. 82, 121012.

Gao, Z.B., Liu, D., Tomanek, D., 2018b. Two-dimensional mechanical metamaterials with unusual Poisson ratio behavior. Phys. Rev. Appl. 10, 064039.

Geim, A.K., Novoselov, K.S., 2007. The rise of graphene. Nat. Mater. 6, 183–191.

Gibson, L.J., Ashby, M.F., 1999. Cellular solids: Structure and Properties. Cambridge university press.

Gibson, L.J., Ashby, M.F., Schajer, G.S., Robertson, C.I., 1982. The mechanics of two-dimensional cellular materials. Proc. R. Soc. A 382, 25–42.

Gogotsi, Y., Anasori, B., 2019. The rise of Mxenes. ACS Nano 13, 8491–8494.

Greaves, G.N., Greer, A.L., Lakes, R.S., Rouxel, T., 2011. Poisson's ratio and modern materials. Nat. Mater. 10, 823–837.

Grima, J.N., Grech, M.C., Grima-Cornish, J.N., Gatt, R., Attard, D., 2018. Giant auxetic behaviour in engineered graphene. Ann. Phys. 530, 1700330.

Grima, J.N., Winczewski, S., Mizzi, L., Grech, M.C., Cauchi, R., Gatt, R., Attard, D., Wojciechowski, K.W., Rybicki, J., 2015. Tailoring graphene to achieve negative Poisson's ratio properties. Adv. Mater. 27, 1455–1459.

Haastrup, S., Strange, M., Pandey, M., Deilmann, T., Schmidt, P.S., Hinsche, N.F., Gjerding, M.N., Torelli, D., Larsen, P.M., Riis-Jensen, A.C., Gath, J., Jacobsen, K.W., Mortensen, J.J., Olsen, T., Thygesen, K.S., 2018. The computational 2D materials database: High-throughput modeling and discovery of atomically thin crystals. 2D Mater. 5, 042002.

Hall, L.J., Coluci, V.R., Galvao, D.S., Kozlov, M.E., Zhang, M., Dantas, S.O., Baughman, R.H., 2008. Sign change of Poisson's ratio for carbon nanotube sheets. Science 320, 504–507.

Huang, C., Chen, L., 2016. Negative Poisson's ratio in modern functional materials. Adv. Mater. 28, 8079–8096.

Jiang, J.W., Chang, T., Guo, X., Park, H.S., 2016. Intrinsic negative Poisson's ratio for single-layer graphene. Nano Lett. 16, 5286–5290.

Jiang, J.W., Park, H.S., 2014. Negative Poisson's ratio in single-layer black phosphorus. Nat. Commun. 5, 4727.

Jiang, J.W., Park, H.S., 2016. Negative Poisson's ratio in single-layer graphene ribbons. Nano Lett. 16, 2657–2662.

Khaledialidusti, R., Anasori, B., Barnoush, A., 2020. Temperature-dependent mechanical properties of $Ti_{n+1}CNO_2$ (n = 1, 2) mxene monolayers: a first-principles study. Phys. Chem. Chem. Phys. 22, 3414–3424.

Lakes, R., 1987. Foam structures with a negative Poisson's ratio. Science 235, 1038–1040.

Lakes, R., 1993. Materials with structural hierarchy. Nature 361, 511–515.

Lempriere, B.M., 1968. Poisson's ratio in orthotropic materials. AIAA J. 6, 2226–2227.

Lv, C., Krishnaraju, D., Konjevod, G., Yu, H., Jiang, H., 2014. Origami based mechanical metamaterials. Sci. Rep. 4, 5979.

Mannix, A.J., Zhou, X.F., Kiraly, B., Wood, J.D., Alducin, D., Myers, B.D., Liu, X., Fisher, B.L., Santiago, U., Guest, J.R., Yacaman, M.J., Ponce, A., Oganov, A.R., Hersam, M.C., Guisinger, N.P., 2015. Synthesis of borophenes: anisotropic, two-dimensional boron polymorphs. Science 350, 1513–1516.

Mortazavi, B., Shahrokhi, M., Makaremi, M., Rabczuk, T., 2017. Anisotropic mechanical and optical response and negative poisson's ratio in Mo_2C nanomembranes revealed by first-principles simulations. Nanotechnology 28, 115705.

Muskhelishvili, N.I., 1953. Some Basic Problems of the Mathematical Theory of Elasticity. Noordhoff, Groningen.

Nye, J.F., 1957. Physical Properties of crystals: Their representation By Tensors and Matrices. Clarendon Press.

Pratapa, P.P., Liu, K., Paulino, G.H., 2019. Geometric mechanics of origami patterns exhibiting Poisson's ratio switch by breaking mountain and valley assignment. Phys. Rev. Lett. 122, 155501.

Puigdollers, A.R., Alonso, G., Gamallo, P., 2016. First-principles study of structural, elastic and electronic properties of α-, β- and γ-graphyne. Carbon N Y 96, 879–887.

Qin, H., Sun, Y., Liu, J.Z., Li, M., Liu, Y., 2017. Negative Poisson's ratio in rippled graphene. Nanoscale 9, 4135–4142.

Schenk, M., Guest, S.D., 2013. Geometry of miura-folded metamaterials. Proc. Natl. Acad. Sci. USA 110, 3276–3281.

Shao, Q., Li, R.S., Yue, Z.G, Wang, Y.L., Gao, E.L., 2021. Data-driven discovery and understanding of ultrahigh modulus crystals. Chem. Mater. 33 (4), 1276–1284. https://doi.org/10.1021/acs.chemmater.0c04146.

Shivers, J.L., Arzash, S., MacKintosh, F.C., 2020. Nonlinear Poisson effect governed by a mechanical critical transition. Phys. Rev. Lett. 124, 038002.

Taylor, M., Francesconi, L., Gerendas, M., Shanian, A., Carson, C., Bertoldi, K., 2014. Low porosity metallic periodic structures with negative Poisson's ratio. Adv. Mater. 26, 2365–2370.
Thorpe, M.F., Jasiuk, I., 1992. New results in the theory of elasticity for two-dimensional composites. Proc. R. Soc. A 438, 531–544.
Ting, T.C.T., 2004. Very large Poisson's ratio with a bounded transverse strain in anisotropic elastic materials. J. Elast. 77, 163–176.
Ting, T.C.T., Barnett, D.M., 2005. Negative Poisson's ratios in anisotropic linear elastic media. J. Appl. Mech. 72, 929–931.
Ting, T.C.T., Chen, T.Y., 2005. Poisson's ratio for anisotropic elastic materials can have no bounds. Q. J. Mech. Appl. Math. 58, 73–82.
Wan, J., Jiang, J.W., Park, H.S., 2017. Negative Poisson's ratio in graphene oxide. Nanoscale 9, 4007–4012.
Wang, H., Li, X., Li, P., Yang, J., 2017. Delta-phosphorene: a two dimensional material with a highly negative Poisson's ratio. Nanoscale 9, 850–855.
Wei, Z.Y., Guo, Z.V., Dudte, L., Liang, H.Y., Mahadevan, L., 2013. Geometric mechanics of periodic pleated origami. Phys. Rev. Lett. 110, 215501.
Wen, Y., Gao, E., Hu, Z., Xu, T., Lu, H., Xu, Z., Li, C., 2019. Chemically modified graphene films with tunable negative Poisson's ratios. Nat. Commun. 10, 2446.
Yang, J.T., Wang, Y., Li, Y.F., Gao, H.J., Chai, Y., Yao, H.M., 2018. Edge orientations of mechanically exfoliated anisotropic two-dimensional materials. J. Mech. Phys. Solids 112, 157–168.
Yasuda, H., Yang, J.J.P.r.l., 2015. Reentrant origami-based metamaterials with negative Poisson's ratio and bistability. Phys. Rev. Lett. 114, 185502.
Zhang, S., Zhou, J., Wang, Q., Chen, X., Kawazoe, Y., Jena, P., 2015. Penta-graphene: a new carbon allotrope. Proc. Natl. Acad. Sci. 112, 2372–2377.